LA-UR-18-21265
Approved for public release; distribution is unlimited.

Title: In-Situ Printing of Conductive Polylactic Acid (cPLA) Strain Sensors Embedded into Additively Manufactured Parts using Fused Deposition Modeling

Author(s): Ouellette, Brittany Joy

Intended for: Masters Thesis

Issued: 2018-02-16

UNIVERSITY OF CALIFORNIA, SAN DIEGO

In-Situ Printing of Conductive Polylactic Acid (cPLA) Strain Sensors Embedded into Additively Manufactured Parts using Fused Deposition Modeling

A thesis submitted in partial satisfaction of the requirements
for the degree of Master of Science

in

Structural Engineering with Specialization in Structural Health Monitoring,
Prognosis and Validated Simulations

by

Brittany Joy Ouellette

Committee in charge:

Professor Michael D. Todd, Chair
Professor Charles Farrar
Professor Hyonny Kim

2018

The Thesis of Brittany Joy Ouellette as it is listed on UCSD Academic Records is approved, and it is acceptable in quality and form for publication on microfilm and electronically:

Chair

University of California, San Diego
2018

TABLE OF CONTENTS

LIST OF ABBREVIATIONS

SHM	Structural Health Monitoring
GF	Gauge Factor
PLA	Poly-Lactic Acid
cPLA	Conductive Poly-Lactic Acid
AM	Additive Manufacturing
DAQ	Data Acquisition
LV	LabVIEW
STL	Sterolithography
FDM	Fused Deposition Modeling
DIC	Digital Image Correlation
N	newtons
ROI	Region of Interest
ABS	Acrylonitrile Butadiene Styrene
ROI	Region of Interest

LIST OF SYMBOLS

ε	Strain
ρ	Density
A	Cross-sectional Area
r	Resistivity
R	Resistance
R_0	Resting Resistance
ΔR	Change in Resistance from R_0
σ	Stress
E	Young's Modulus
Ω	Ohms
L	Length of gauge wire

LIST OF FIGURES

LIST OF TABLES

ACKNOWLEDGEMENTS

I would like to acknowledge Professor Michael Todd for his support as the chair of my committee and also in conjunction with Professor Charles Farrar: for their tireless efforts in restarting the distance-learning program between UCSD and LANL, for not just myself, but others in a similar position, looking to advance their education and research ability.

To Professor Hyonny Kim, while meeting with only days before I moved to New Mexico, you agreed to try remote learning, which meant adjusting your classroom and lessons to accommodate me. I truly appreciate the extra effort you put forth in allowing this degree to become a reality.

Yvonne Wollmann, Ellie Vigil, Christine Starr, and Gabrielle Coulousi: your organization and support are the backbone to this master's program.

I would like to acknowledge the LANL cohort students, for your camaraderie. Without you all, long nights would be much longer, and classes wouldn't be as entertaining. I am lucky to call you coworkers, colleagues and friends. I look forward to working with you for many years.

Dad, thank you for all those years of encouragement; both about engineering and life. I appreciate the time I spent as young girl soldering with you, and going on road trips and hikes. Mom, thank you for always having my scholarly and artistic interests at heart; and also for instilling a work ethic in me that is borderline scary at times. Brooke, thanks for being my best friend growing up, and the test pilot to many our pillow forts, stair-toboggan sleds and go-carts. Your achievements in your geology career have inspired me to pursue this masters.

To my wonderful husband Scott, you have encouraged me and have been my rock through the entire program and our move to New Mexico. You believed in me even when I thought I was in over my head. I cannot thank you enough for your unwavering support and love.

The Abstract, and Chapter 1 through 4, in part, have been published in the manuscript, 11th International Workshop on Structural Health Monitoring 2017. Rumley-Ouellette, Brittany J., Wahry, J., Baker, A., Bernardin, J, Marchi, A., Todd, M. The thesis author was the primary investigator and author of this paper.

ABSTRACT OF THE THESIS

In-Situ Printing of Conductive Polylactic Acid (cPLA) Strain Sensors Embedded into Additively Manufactured Parts using Fused Deposition Modeling

By

Brittany Joy Ouellette

Master of Science in Structural Engineering with Specialization in Structural Health Monitoring, Prognosis and Validated Simulations

University of California, San Diego, 2018

Professor Michael D. Todd, Chair

Additive Manufacturing (AM) technology has been around for decades, but until recently, machines have been expensive, relatively large, and not available to most institutions. Increased technological advances in 3D printing and awareness throughout industry, universities, and even hobbyists has increased demand to substitute AM parts in place of traditionally manufactured (subtractive) designs; however, there is a large variability of part quality and mechanical behavior due to the inherent printing process, which must be understood before AM parts are used for load bearing and structural design

The research detailed in this thesis paper presents a technique to additively manufacture conductive polymer strain sensors into 3D printed polymer-based components in order to measure internal strains. Having the ability to measure internal strains gives researchers a deeper understanding of how this printed material responds to loading, and it would allow end-users the ability to confirm part-to-part prints are straining as expected. Methods to assemble the coupons for data acquisition and unidirectional loading and unloading are also detailed in this report. Several common printing variables are explored in order to understand the effects of user-defined printing parameters on the sensor sensitivity and linearity while subjected to unidirectional tensile loading.

Findings from this study demonstrate a strong correlation between coupon strain and resistance measured from the conductive strain sensor. Although several print variables were explored in this study, the gauge factor, linearity, and repeatability of similar results varied significantly; thus preventing strong correlations between variables and the quality of the conductive strain sensor.

The Abstract, and Chapter 1 through 4, in part, have been published in the manuscript, 11th International Workshop on Structural Health Monitoring 2017. Rumley-Ouellette, Brittany J., Wahry, J., Baker, A., Bernardin, J, Marchi, A., Todd, M. The thesis author was the primary investigator and author of this paper.

Chapter 1

Introduction

In the last few decades, additive manufacturing (AM) capabilities, driven by industrial and consumer demand, have increased significantly leading to extreme technological advances. While there is fervent growth in consumer AM popularity with potential for multiple applications, there is still a vast amount of uncertainty in part-to-part variability between each 3D printer and more specifically with variations in print settings on a given 3D printer. Furthermore, studies have shown that 3D printed components display mechanical properties that are anisotropic [1, 4], with the direction and degree of anisotropy being dependent on build orientation, thus requiring additional understanding of printed components *a priori* to service deployment. Individual part testing and qualification is time-consuming and prohibitively expensive, which necessitates constant or periodic monitoring. Embedding a sensor within a part's geometry without disrupting the mechanical integrity allows for monitoring internal strain responses to ambient loading while being able to retain the part for its intended purpose. Whereas traditionally manufactured parts are monitored by placing commercial strain gauges on the exterior surfaces, often in locations that are difficult to access or sub-optimal for measuring strain fields at potential damage nucleation points. Additional value is placed on the AM fabrication method that allows embedding of sensors internally, with limited impact to mechanical properties and part build time. This allows the possibility for both an inexpensive part qualification testing immediately after fabrication, and informative health monitoring during the lifetime of the part.

The embedded prototype strain sensors presented in this thesis are printed with carbon filler material dispersed into a base thermoplastic and extruded to a given diameter to produce a filament that can be used in fused deposition modeling (FDM). The carbon filler material has a negligible effect on the overall mechanical properties of the thermoplastic, while simultaneously modifying the electrical conductivity, allowing the material to conduct electricity. Strain sensors produced using this material operate similarly to commercial strain gauges, i.e., as the part is strained by an external mechanical load, the material deformation produces a measureable change in the electrical resistance of the sensor.

The goals of this research are the following: 1) understand the parameters that affect the electrical-mechanical properties of the conductive filament, e.g., gauge geometry design configurations, operational variability, and environmental factors; 2) calibrate the conductive sensors with a gauge factor; and, finally, 3) understand how these variable parameters affect the gauge factor and sensitivity of the designed sensor.

1.1 Related Research

There has been documented research activity of using carbon fibers and carbon-based materials infused into a silicon, or polymeric matrix and observing the electrical resistance response to material strain [3, 7, 14, 15] A significant portion of previous research was focused toward bio-medical applications, such as medical implants, or for applications that are not concerned with structural integrity of the host object, but more focused on high strain applications [7]. However, research activity in the effort of integrating carbon-doped strain sensors into the FDM printing process remains quite novel. The research findings of Muth et al. [7] with embedded carbon ink yields good correlation of resistance to strain but is likely to

be incompatible with common plastic AM materials such as PLA (polylactic acid) and ABS (acrylonitrile butadiene styrene). Furthermore, their paper also studies the effects of print speed on the electro-mechanical response: faster print speeds created a sensor with a smaller cross-sectional area and a larger sensitivity to strain than those sensors printed with slower print speeds. The research from Sbriglia et al. [10] integrates embedded piezoelectric accelerometers into PLA parts; however, the sensors are not of the same material as the part and require manual installation during the part build process. By co-printing two materials into one part, a strain reading can be obtained through the conductive polylactic acid (cPLA) filament material with minimal effects towards the mechanical properties of the host PLA part.

There have also been studies in understanding the complexities of conductive elastomer behavior subject to uniaxial loading. Bergstrom and Boyce [5] studied the effects of strain-rate dependencies of elastomers with various fill percentages of carbon black, and found that the elastomer (Chloroprene rubber) showed significant amounts of hysteresis for cyclic loading, but that the amount of carbon black filled rubber did not strongly influence the hysteresis response. Other researchers such as Kost et al. and Stubler et al. [6, 12] have focused on the resistivity change in carbon black particle configuration during the elongation process; specifically the dependency to strain, and separate studies of resistance behavior with respect to loading cycles over a longer time duration. Stubler [12] investigated the strain softening properties of filled elastomers using the dynamic flocculation model which studies the molecular bonds of filler particles.

Gooding and Fields' [2] recent published work closely relates to the experimental approaches taken in this thesis. Gooding and Fields' paper and the work in this thesis differ

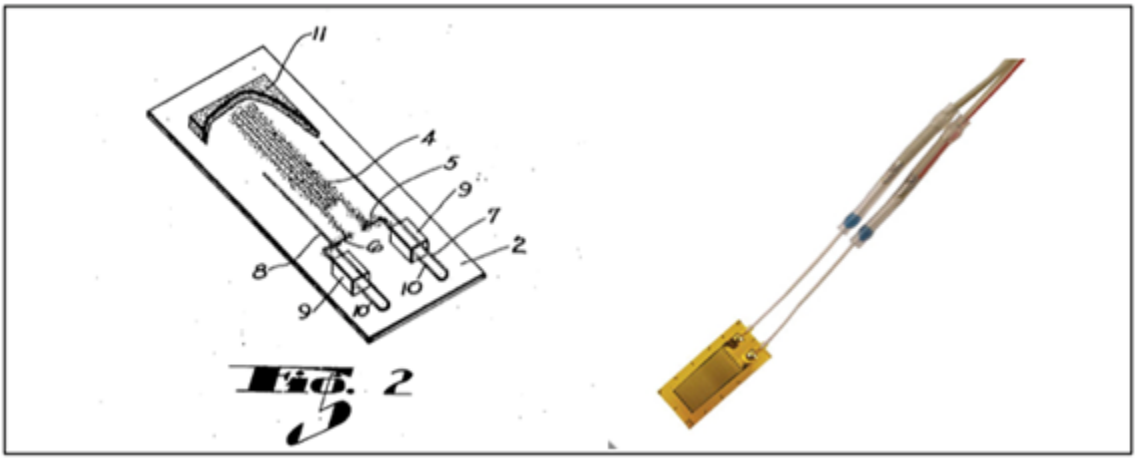

Figure 1: Examples of strain gauges. LHS is from Ruge's patent in 1944 [11]. RHS is a commercial linear strain gauge made by Omega [8]. This is similar to the strain gauge used in this study for developing GF.

from one another in the chosen variables as well as post processing methods. First, this paper focuses primarily on commonly adjusted user-controlled print parameters in polymer AM machines, while Gooding and Fields [2] studies the effects of the geometry of the strain sensor. Second, this thesis attempts to define a gauge factor (GF) and other characteristics from each sample. Although the approach of these two works are similar, much can be gleaned from the differences each author has chosen to focus on, and greater understanding of AM strain sensors can be realized through the combined efforts.

1.2 Strain Gauge History and Design

The common commercial strain gauge was independently developed by Simmons and Ruge [17] and is a design consisting of a long, thin wire (typically made from the copper-nickel alloy commonly referred to as Constantan) set in a switch-back, or “serpentine” pattern to form a grid with a relatively short gauge length, compared to the overall wire length. The metallic “grid” is then mounted to a thin paper backing that is used to keep the gauge design stable, and

as an interface to bond the strain gauge to the material sample for testing. This serpentine geometry allows for a relatively sensitive strain measurement from resistance changes in the strain gauge.

Equation (1) below relates the resistance (ohms) to the geometric factors and material properties of the gauge: resistance (R) is proportional to the material resistivity (r) of the wire, multiplied by the full length of the wire (L), divided by the cross-sectional area (A) of the wire. When the material is tested under uniaxial tensile load, the entire foil is elongated, causing the length to increase and, due to Poisson effects, the cross-sectional area of the wire to decrease. Since the foil material is constant, the resistance increases. Under compressive loading, conversely, the measured resistance decreases.

$$R = \frac{rL}{A} \qquad (1)$$

Understanding the geometric gauge parameters that affect measured resistance is important in determining the shape of the strain sensor. Because this switchback geometry increases the sensitivity to resistance change in a small footprint on the coupon, a similar geometry was used for the AM test specimens. Another geometry was also considered for simplicity and to determine if alternative design geometries of the strain sensors would obtain a more sensitive or stable resistance measurement.

Commercial (grid style, paper backed) strain gauges are more common and undergo quality-assurance testing to confirm accuracy; however, they are still prone to several issues. Some of the established concerns with the use and implementation of these gauges are that they

are easily prone to alignment error, damage, and delamination when handling care is not taken, localized stresses due to reinforcement of strain gauge area, adhesive incompatibility, and sensitivity to prolonged environmental exposure. If embedded fiber optics or other sensors are used, there is a concern that the gauges will reduce the mechanical integrity of the part or cause premature delamination of composite materials. Additively manufactured strain sensors will offer more options for strain measurement, including the substantial benefit of embedding strain sensors during the build, which provides novel strain information within the cross-section of the part.

1.3 Gauge Factor

The gauge factor of a strain gauge describes the relationship between the sensitivity of the measured resistance change with respect to physical material strain. Equation 2 below shows the relationship among these three entities. In a conventional strain gauge, an established and published GF is used as a conversion factor to convert measured resistance change (or voltage change in most commercial gauges) to measured material strain (ε). Most metallic-based foil strain gauges will have a gauge factor around 2.0, but GFs can vary widely depending on the type of foil material used. The gauge factor value is considered a sensitivity factor, thus strain gauges with larger GF values return a larger resistance change than a smaller GF for the same given strain. For this reason, a larger gauge factor can allow the user to detect smaller strains when the data acquisition system is limited in measuring small resistance changes.

$$GF = \frac{\left(\Delta R / R_0\right)}{\varepsilon} \qquad (2)$$

Chapter 2 of this thesis introduces the reader to the FDM printing process, sample design and variables explored. Chapter 3 details the experimental set-up and data acquisition approach used throughout the study. Chapter 4 reviews the acquired data, post processing steps and results of the gauge factor and stability of the sensor design. This study reviews common user-controlled parameters in the FDM print process and how much effect they have on the sensitivity of the strain sensor design. Results show that not one parameter is responsible for a direct change in the sensor quality, and that other factors of the print process are responsible for variations in the strain sensor.

The Abstract, and Chapter 1 through 4, in part, have been published in the manuscript, 11th International Workshop on Structural Health Monitoring 2017. Rumley-Ouellette, Brittany J., Wahry, J., Baker, A., Bernardin, J, Marchi, A., Todd, M. The thesis author was the primary investigator and author of this paper.

Chapter 2

AM Printing Design

2.1 Fused Deposition Modeling Process

All samples in this study were additively manufactured using fused deposition modeling (FDM) machines of three different make/models: Rostock V2 delta printer, LulzBot TAZ5, and LulzBot TAZ6 3D printers. The FDM process involves feeding thermoplastic filament into a hot metallic enclosure which heats the material beyond the glass transition temperature, and extrudes the material through a nozzle to deposit the material on a support plate or "print bed" in a path based on the provided part design geometry. The first layer of extruded filament bonds to the build plate and rapidly coalesces to a solid. Another extrusion trace is placed adjacent to the previous one to bond and solidify. Once the first layer is extruded, depending on the printer type, either the build plate lowers slightly or the nozzle raises in order to deposit the next layer without much interference. The process is continued until the full part geometry is printed. Figure 2 and Figure 3 are displayed below to help visualize the FDM process. Figure 3 shows the TAZ6 printer finishing the first few layers of a sample print.

The LulzBot printers were outfitted with a dual material nozzle extruder in order to seamlessly manufacture both regular PLA and conductive PLA materials in the same part without pausing the build to exchange filament reels, as is the standard procedure for a single extruder nozzle. The LulzBot 5 and 6 printer nozzles perform movement in the X-Z plane, while the support plate is movable in the Y axis.

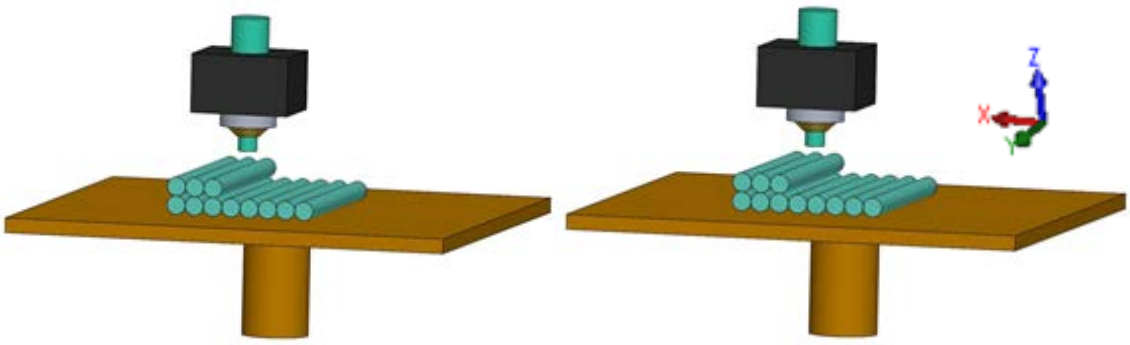

Figure 2: Example schematic of the FDM process. PLA filament is extruded and placed on the print bed where it solidifies in place. Several extrusions are bonded while hot to form individual layers of the part. LHS is a cross-sectional view to show the filament flow.

The Rostock V2 does not have dual extruder nozzles, thus requiring a pause in the print to switch filament reels; however, its overall quality of print was preferred to that of the TAZs. The Rostock differs from the TAZ in that the nozzle is mounted and able to slide and rotate against three vertical posts; this allows for the build plate to remain stationary. Unfortunately, due to safety issues with this particular version of the Rostock, further samples for this research were printing using the TAZ printers. Although using different printers was not considered in the beginning concept for this study, reviewing the effects (if any) on the strain sensor printed from different manufacturers and printer models will aide in further understanding of implementing an effective strain sensor.

2.2 Coupon Geometric Design

The overall design of the test specimen was designed using SolidWorks computer aided design (CAD) software and consists of two parts, or “bodies”, which corresponds to the two different materials used for the coupon samples. The first part is a thin rectangular block with the overall dimensions of the sample used for all tests in this study: 101.6 mm x

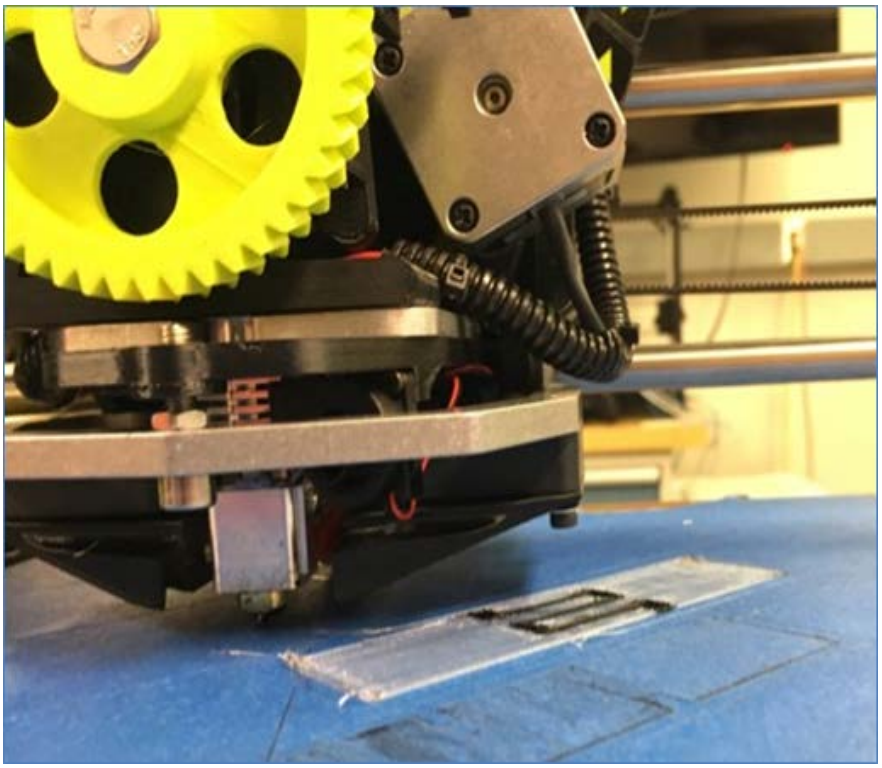

Figure 3: TAZ 6 dual extruder in the middle of printing a sample. Two nozzles are used, and switch on and off depending on the design material.

25.4 mm x 2 mm (l x h x w). The second body serves as the design for the strain sensor; this design is similar to that of the traditional serpentine strain gauge design as mentioned in section 1.2, but simplified with print quality in mind given the limited spatial resolution of the AM machines. Thus, the number of switch-backs was drastically reduced. These two bodies were assembled in SolidWorks to define the full specimen geometry and then converted to a stereolithography (STL) file to be co-printed in the same AM build (see Figure 4). The strain sensor body is almost fully embedded into the regular PLA part with the exception of two attachment pads, which are printed through the entire sample thickness (shown in a darker black in Figure 5 and Figure 6). These conductive pads serve as attachment locations for lead wires, and will be discussed in detail later in this paper.

Figure 4: Workflow diagram from concept design through 3D print.

All but a single coupon were manufactured using the geometric strain sensor design described in the above paragraph and shown in Figure 6 (top). A second design of a simple linear geometry as shown in Figure 6 (bottom) was chosen as an alternative strain sensor design to determine whether this shape would have an effect on the gauge factor, sensitivity or linearity of the sensor.

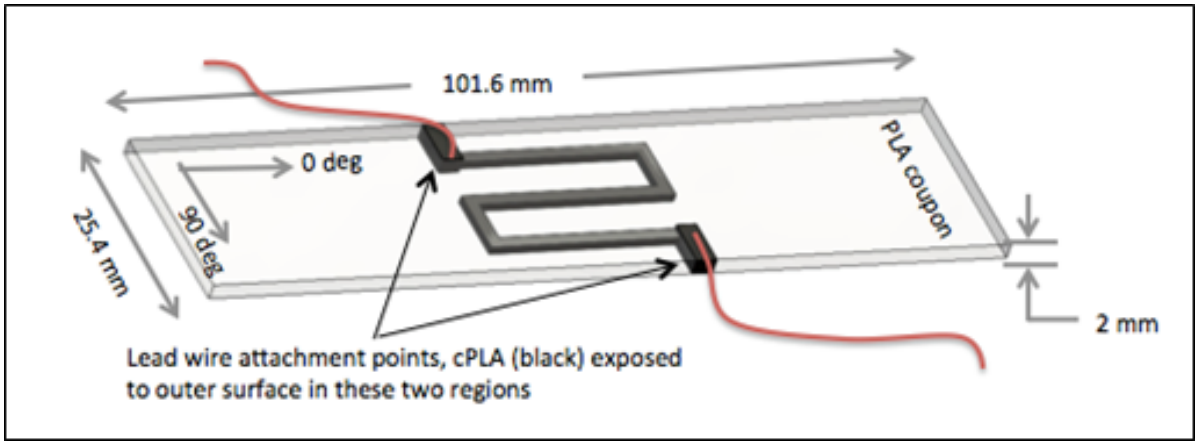

Figure 5: Typical S-gauge coupon design. The cPLA strain sensor is entirely embedded into the regular PLA (clear) coupon except for two small areas where leads are attached and connected to measure sensor resistance.

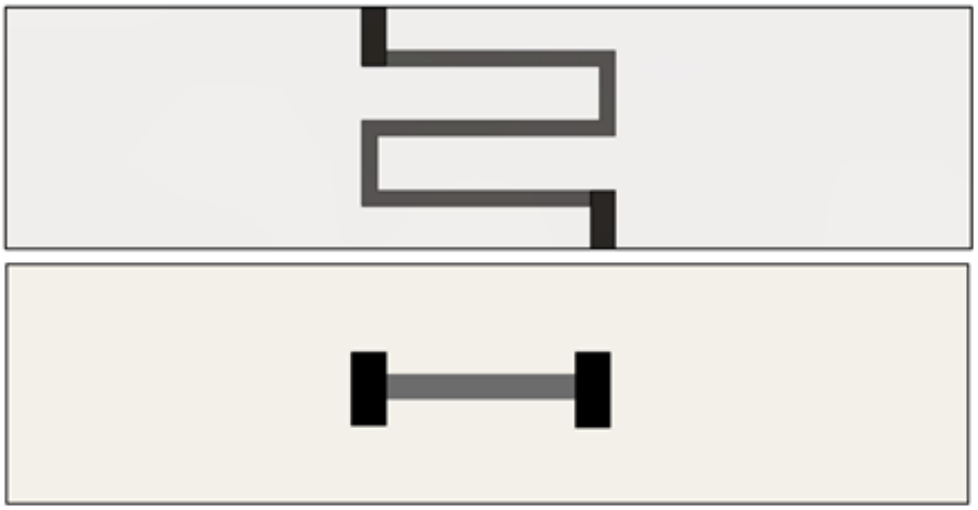

Figure 6: (top) Schematic of serpentine style strain sensor, and (bottom) simplified linear strain sensor

2.3 Additive Manufacturing Process and Parameters Explored

There are a multitude of parameter and configuration settings when printing using LulzBot machines. Many variables for this study were kept constant either from previous knowledge on part quality or for test matrix simplicity. The parameters that were selected to be varied include:

- print speed
- layer height
- print bed temperature
- nozzle temperature
- 3D printer used

Additional known parameters also required adjustment in order to ensure good part quality, or in certain cases, to prevent print failures. These parameters include minor

adjustments to the nozzle flow percent, infill density percent, and user-defined filament diameter. Flow percent is a value that changes the amount of material pushed through the nozzle. Infill density percent is related to the density of extrusions needed to fill the part. A much lower infill density value will enable the program to build a honeycomb type pattern inside the perimeter of the part, and is usually used in order to save print time or material, but is not recommended for structural components. For the printed parts in this research, the goal is to obtain a fully dense part, which can be achieved by using values around 70-100% infill density. Too large of fill percentage can actually reduce the quality of the print by attempting to extrude material for which there may not be space, causing clogs in the nozzle and uneven extrusions. Lastly, the defined filament diameter can be adjusted to better calibrate the length of material extruded for the design. If the filament diameter is less than the default, lowering this value will extrude more material length to make up for the loss in volume. These three parameters are still technically user parameters that are easily adjustable on the TAZ models; however, they were done solely to increase print quality, or to prevent printing failure. An adjustment to any one of these parameters usually requires an additional adjustment to one or both of the others. A further study could be developed to determine the effects of these parameters.

Table 1 shows the parameters tested for all samples. The test matrix for this study initially sought to test a larger range of values for the parameters tested, but once the printing process began, deviating too much from the suggested print settings often yielded parts with poor surface quality or parts that outright failed during the print. Additionally, adjustment of one parameter sometimes required the adjustment to a few more obscure variables in order to obtain a quality print. All coupons were examined and had a smooth surface finish, with no

visual signs of a poorly fabricated part. Although these parts have the same design file used to print, the strain sensor geometry appears different upon visual inspection. Since this study has varying values for print speed and temperature at which the material is extruded, it is expected that there will be variation in the appearance of the samples. This study is to determine whether these parameters have a quantifiable impact on the performance of the strain sensor.

Table 1: Printing parameters for all 29 samples.

Sample #	Organizing group SET	Printer	Layer Height (mm)	Nozzle 1 Temp (°C)	Nozzle 2 Temp (°C)	Build Plate Temp (°C)	Print Speed (mm/sec)	density (%)	Flow (%)	Nozzle 1 diameter change	Nozzle 2 diameter change
1	1	Rostock	0.2	210	210	60	40	100	NA	None	None
2	1	Rostock	0.2	210	210	60	40	100	NA	None	None
3	2	TAZ 5	0.2	208	215	70	20	70	100	None	None
4	2	TAZ 5	0.2	208	215	70	50	70	100	None	None
5	2	TAZ 5	0.2	208	215	70	50	70	100	None	None
6	2	TAZ 5	0.2	208	215	70	50	70	100	None	None
7	2	TAZ 5	0.2	208	215	70	50	70	100	None	None
8	3	TAZ 5	0.2	208	215	70	50	70	100	None	None
9	4	TAZ 6	0.25	208	205-208	50	NA	70	100	None	None
10	4	TAZ 6	0.25	208	205-208	50	NA	70	100	None	None
11	4	TAZ 6	0.2	208	208	50	NA	70	100	None	None
12	4	TAZ 6	0.2	208	208	50	NA	70	100	None	None
13	4	TAZ 6	NA	NA	NA	NA	NA	NA	100	None	None
14	4	TAZ 6	NA	NA	NA	NA	NA	NA	100	None	None
15	4	TAZ 6	NA	NA	NA	NA	NA	NA	100	None	None
16	5	TAZ 6	0.2	210	210	32/NA	50	NA	100	3.35	None
17	5	TAZ 6	0.2	210	210	32/NA	50	NA	100	3.35	None
18	5	TAZ 6	0.2	210	210	32/NA	50	NA	100	3.35	None
19	5	TAZ 6	0.2	210	210	32/NA	50	NA	100	3.35	None
20	6	TAZ 6	0.2	210	210	33	50	70	100	3.35	None
21	6	TAZ 6	0.2	210	210	33	50	70	100	3.35	None
22	6	TAZ 6	0.2	210	210	33	50	70	100	3.35	None
23	6	TAZ 6	0.2	210	210	33	70	70	100	3.35	None
24	6	TAZ 6	0.2	210	210	33	70	70	100	3.35	None
25	6	TAZ 6	0.2	215	210	33	50	70	90	3	2.75
26	6	TAZ 6	0.2	212	210	33	20	70	90	3	2.75
27	6	TAZ 6	0.2	212	210	33	50	70	90	3	2.75
28	6	TAZ 6	0.25	212	210	33	50	70	90	3	2.8
29	6	TAZ 6	0.25	210	205	33	50	70	90	3	2.85

2.4 Coupon Assembly

All test coupons required the installation of two wire leads in order to acquire resistance measurements during testing. A soldering iron was used to conductively heat the stripped wire leads and melt through a portion of the exposed cPLA conductive pads. The soldering iron was used to push the softened cPLA around the wire-end to ensure good contact. The other end of each wire was stripped in order to easily attach the multimeter test leads to each sample. The next step was to adhere a linear gauge commercial strain gauge (Omega KFH-10-120-C1-11L3M3R 10mm gauge length, 3-wire) to the smoother side, or print-bed side of the sample in the region occupied by the embedded strain sensor. The sample was cleaned lightly with isopropanol alcohol using a Kimwipe and allowed to dry. Next, Kapton tape was first positioned to the strain gauge to aid in gauge alignment to the sample (see Figure 7). A thin coat of Cyanoacrylate was applied to the commercial strain gauge. The gauge and tape were then laid onto the coupon; light and constant pressure was applied to the gauge using the tape as a barrier. Although some degree of added measurement noise and error will be included from the usage of commercial strain gauges to derive the gauge factor of the printed conductive strain sensor, it was found that the commercial gauge was still best tool for a direct method of deriving the prototype strain sensor GFs, and also to serve as a baseline for strain comparison at any given time during the load cycle(s).

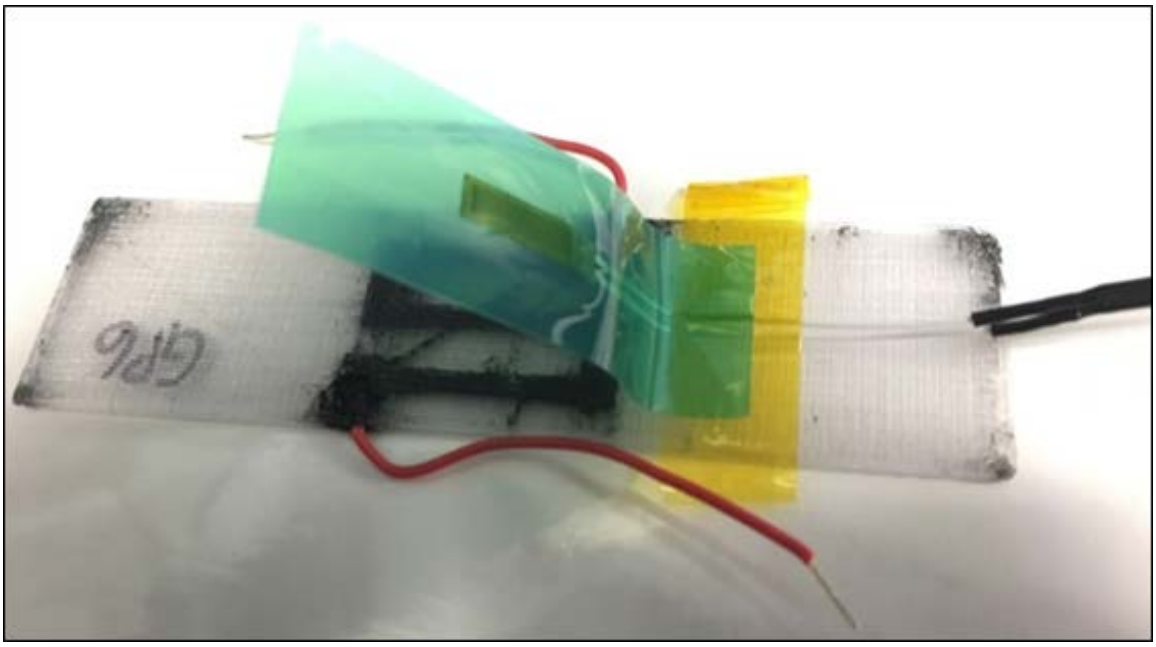

Figure 7: Kapton tape used in assembly for several reasons: 1) to pre-align the commercial strain gauge, 2) aids in adhesive flow for adhering the gauge to the coupon. 3) It also provides a barrier so that pressure can be applied while bonding.

The Abstract, and Chapter 1 through 4, in part, have been published in the manuscript, 11th International Workshop on Structural Health Monitoring 2017. Rumley-Ouellette, Brittany J., Wahry, J., Baker, A., Bernardin, J, Marchi, A., Todd, M. The thesis author was the primary investigator and author of this paper.

Chapter 3

Methodology

3.1 Experimental Layout

This section reviews the structure and purpose of each of the four types of tests performed during this study. The primary focus of this research is on the correlation between the coupon strain and the resistance readings from the conductive strain sensor. This experimental setup is defined first in the section below. The following three tests were performed to a much lesser extent, but they provide valuable information that would affect the implementation of this type of strain sensor into a product.

3.1.1 Tension Test for Strain-Resistance Comparison and Determining Gauge Factor

The two lead wires from the coupons were attached to a Fluke 8845A multimeter, which measured resistance of the strain sensor with a sampling rate of 0.5-1 sample/second. A different option using National Instruments (NI) cRio DAQ cards were considered part way during the data collection, but the maximum resistance measurement capability stated by NI was lower than several of the coupons' resting resistance measurements. The 3-wire commercial strain gauge lead wires were connected into a Micro-Measurements P3 strain indicator and recorder. For each test, resting resistance was captured for several recording samples prior to adding load.

Two load frames were used throughout this study to preform tension cycle of loading and unloading along length of each coupon. The Mark-10 ESM 301L stand and a MecMesin Multi-test 10-i test stand were used to supply a controlled loading and unloading cycle of

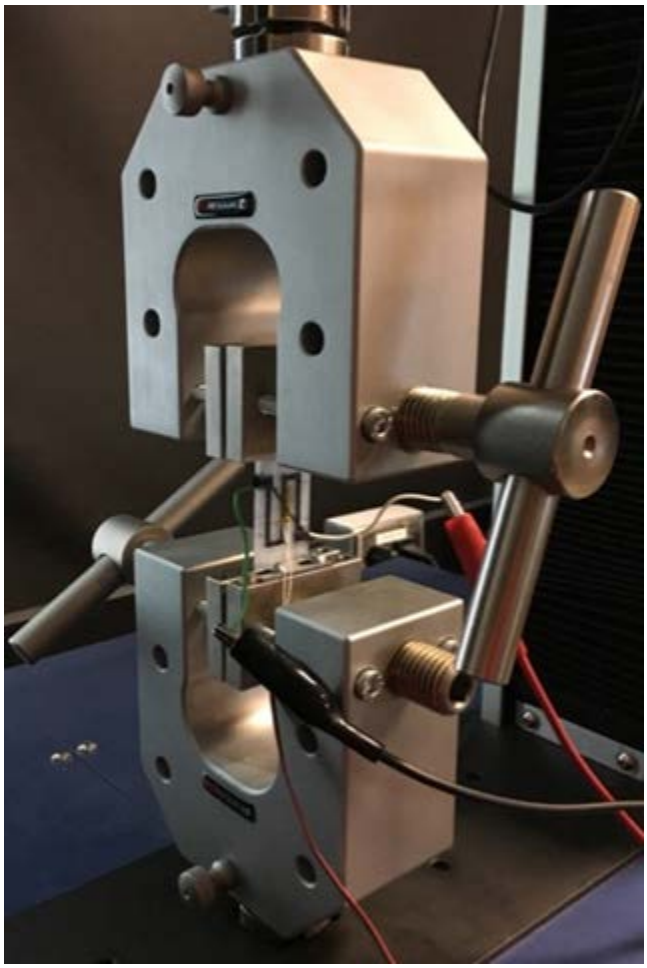

Figure 8: Coupon installed into MecMesin test stand and strain sensor leads hooked up to Fluke 8845A multimeter. Commercial strain gauge also shown near center of strain sensor.

tension force on the coupons. Extension rates were kept low (0.5-1 mm/min) for sampling rate limitations. The MecMesin load frame system contained specimen grips that could be manually aligned, but the load cell was designed for loads much larger than the loads required for testing and the lower limit on displacement rate was too fast for the DAQ system to capture enough samples during 1 cycle of loading and un-loading. The Mark-10 load stand was preferred in that the load cell on this stand was more suited to load for this test and the displacement rates available were low enough to allow for a larger collection of data points per load cycle. The

concern with the Mark-10 test stand is that the grips were misaligned, with no possibility of readjustment, allowing for possible loading conditions other than pure tension.

Most initial tensile testing was completed within three to five cycles, and later testing was performed with only 1 or 2 cycles. More cycles were performed in earlier tests as means to collect more data points per coupon, but evaluation of the results was limited to the first cycle. Hysteresis was present in the results and was also mentioned in several similar articles relating to similar polymer based strain sensors [2, 3, 5, 7, 9, 12]. This will be evaluated in detail in the results section.

Although the force applied to the coupon was not used in the data analysis, the maximum load, or peak load for the testing cycles were kept low enough avoid failure and to avoid any higher strain behavior that may affect results. Rostock coupons were loaded to approximately 220 newton (N), while maximum loading on TAZ coupons was in the range of 90 – 133 N.

3.1.2 Basic Stiffness Comparison Test

Before initiating this detailed parametric study, there were concerns as to whether the strain sensor would weaken the host parts that they would be embedded within. A cursory uniaxial tensile load study was performed directly comparing samples with embedded printed strain sensors, surface printed strain sensors, and coupons without strain sensors. Force and displacement data were collected during each test to determine whether the embedded strain sensor coupons performed similar to the non-embedded coupon types for loads comparable to testing loads in this study. Although this test captured sample extension response under relatively small loads, additional testing

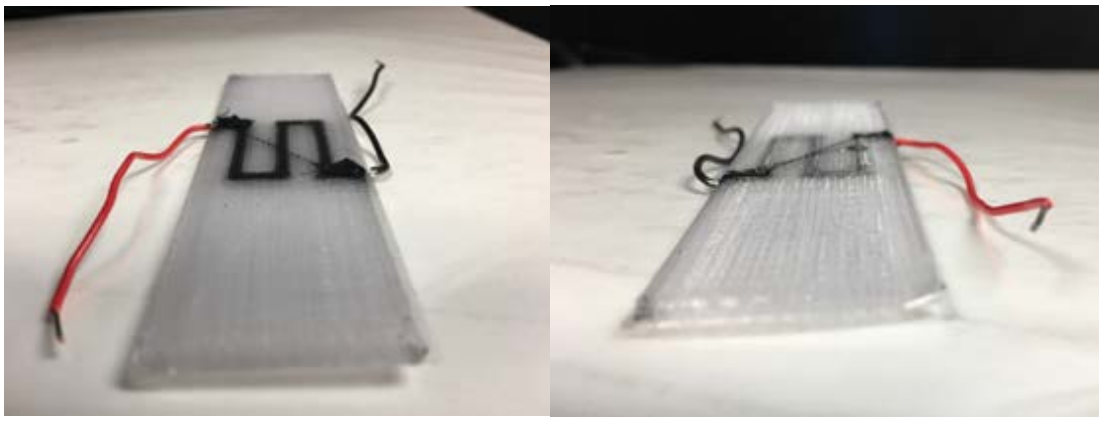

Figure 9: Photos of each side of one sample. The print-bed surface side is shown on the left, and the free surface side is shown on the right.

would eventually be required to confirm that the failure strength is not greatly reduced from the incorporation of the strain sensors.

3.1.3 Temperature- Resistance Comparison Tests

While performing initial testing (for determining GF), it was discovered that the resistance measurements were non-stationary even while the samples were at rest. A few initial experiments were run to determine whether these fluctuations were dependent on the laboratory room temperature, or were from other sources such as self-heating. These preliminary tests consisted of measuring resistance of the strain sensor and coupon surface temperature from a thermocouple over a longer duration of time. The original data collected was through manual recordings of both resistance and temperature, but this temperature dependency was later explored in detail under larger temperature variations by Wahry et al. [13]. Although investigated more thoroughly in [13], a recreation of the initial room temperature vs. resistance was recorded for approximately 10-minute segments and shown in the results section. This information is documented in order to show the temperature dependent behavior of the strain sensor operating in a controlled laboratory environment.

3.1.4 Print Surface Strain Dependencies & Digital Image Correlation (DIC) Tests

As mentioned before, the Mark-10 test stand grips were misaligned with no method of adjustment. Another interesting observation is that each side of the sample has a different surface finish; the print-bed surface is smoother and more translucent, where the free side of the sample usually is slightly rougher to the touch, and with a slightly opaque appearance.

To understand the degree of influence of these two observations on the test measurements, two identical strain gauges were adhered to each side of a sample coupon and tested under tensile load. Once the test was performed, the coupon was flipped so that the back surface now faced forward. The results of these tests were not as expected, as the amount of strain offset between the two gauges did not simply reverse when the sample was flipped. To better understand whether the results were a factor of grip misalignment or potential strain gauge bonding issues, testing using the MecMesin test stand with a few coupons and Digital Image Correlation (DIC) was performed on one coupon.

Three-dimensional (3D) DIC is a method of simultaneously capturing high-resolution images from two angled cameras on a test specimen that has a high contrast speckle pattern (typically black and white) while the specimen is being loaded or tested. The software then post processes the data and determines strains by tracking small sub-set groups of pixels relative to each pixel's gray-scale value [16].

Only one test was required for MecMesin testing with the sample containing two strain gauges, but to be sure that there was minimal misalignment effects, an additional test was performed with the coupon flipped. Although the MecMesin test stand has the ability to adjust the grips, the additional test was done to confirm any offset in strains value was due to material behavior, and not any test stand bias or misalignment. Two tests were also performed for the

sample tested with DIC; one test with side 1 facing the stationary cameras, the second test was performed after the coupon was flipped so that side 2 was facing the cameras. DIC images were captured throughout the tensile loading and unloading cycle and then post processed with VIC 3D DIC software from Correlated Solutions to determine longitudinal strain.

3.2 Design and Assembly Component Assumptions

3.2.1 Commercial Strain Gauge

Omega 10mm linear strain gauges bonded using Z70 cyanoacrylate were used in order to capture the coupon strain in the region of application. The strain gauge measurements have their own error associated with the foil: the nominal resistance of the gauge is 121.2 Ω with an error of +/- 0.35% and its own gauge factor of 2.06 with an error or +/- 1 %. For this study, the nominal values were used. Although the method of adhesive application and pressure were consistent throughout the entire study, there is likely a range of adhesive bond-line thickness and type of adhesive used, and due to the nature of varying the printing parameters, the overall quality of bond may vary from coupon to coupon.

3.2.2 Assembly of Lead Wires

The lead wires were assembled to the coupons using the same technique throughout the entire study: by use of a soldering iron to heat the lead wire through the conductive PLA attachment pad. Although best efforts were made to keep all cPLA intact, some conductive filament was removed in the process of attempting to compact cPLA around the lead wire. In later coupons, additional cPLA material was heated and added to the conductive pad in order to ensure optimum contact with the wire, and to avoid any adjustment in nominal resistance. At the point, no process was used to verify full contact between the cPLA and lead wires.

3.2.3 Repetition from 3D Printer

The LulzBot TAZ machines do not have the finest spatial resolution of 3D printers on the market, and each require either automatic or manual print bed leveling prior to print. Manual offsets are changeable, and filament can swell over time due to ambient moisture absorption. Many minor non-user controlled changes could have an effect on the final printed item, even if they come from the same design and user defined print parameters. Printer component settling, nozzles clogging, and moisture ingression into the filament are examples of changes within the printer set-up that cannot be fully controlled. Samples from set #5 were printed with the exact same print parameters and within a few days of each other to see if the GF, linearity, and hysteresis results would be closer in value than to the other samples.

3.2.4 Triggering and Recording of Data

Data acquisition for commercial strain gauge strain measurements and strain sensor resistance measurements were taken from the same computer, but not the same triggering software. A scripted algorithm written in Python was used to record resistance measurement from the Fluke multimeter, while the strain indicator unit from Vishay PG uses their own triggering software to record strain. This gives rise to a slight time offset between strain and resistance measurements, and potential errors in determining the gauge factor if any dynamic behavior of the coupon is of the same as the sampling rate.

The Abstract, and Chapter 1 through 4, in part, have been published in the manuscript, 11th International Workshop on Structural Health Monitoring 2017. Rumley-Ouellette, Brittany J., Wahry, J., Baker, A., Bernardin, J, Marchi, A., Todd, M. The thesis author was the primary investigator and author of this paper.

Chapter 4

Experimental Results

Results are discussed in the same order as introduced in the experimental chapter. The first section discusses resting resistance. The second section is devoted to the results and processing of the strain-resistance measurements taken under one cycle of tensile loading. This is the primary focus of this thesis, and additional observations through testing are mentioned in the following sections.

4.1 Strain vs. Resistance Results & Determination of Gauge Factor

4.1.1 Nominal Resistance of Strain Sensor

As explored by Muth et al. [7] resistance of their conductive ink sensor changed depending upon the print speed of the deposition print nozzle. For Muth's study, the nozzle print speed directly affected the thickness of the sensor, and thus an increase in print speed caused an increase in sensor resistance.

For the study presented in this thesis, nominal resting resistance of the strain sensors did not correlate with print speed. The coupons have varying values of nominal resistance (initial resistance prior to loading). Although it is important to note that most of the 29 samples were printed with other varied parameters in addition to the print speed, even those samples that varied the least (other than with print speed) did not show any substantial change or correlation to resting resistance. The main focus of this study is on gauge factors and predicting strains; thus, more testing of print geometries and printing parameters will be required in order to fully understand the factors affecting resting resistance.

4.1.2 Resistance Response to Loading and Gauge Factor Determination

Earlier results from AM coupons printed from the Rostock showed a very strong correlation and consistency between the normalized changes in resistance to strain with limited hysteresis. Coupons from all three machines showed behavior similar to that in Figure 10, where the strain behavior matched with the resistance behavior with respect to time.

The first value extracted from the testing results was the starting resistance, either by taking an average of several resistance measurements prior to loading, or if none were measured, the starting value would be the first recorded resistance value. The first value of interest is the first-cycle gauge factor. As previously mentioned in Section 1.3, the gauge factor depends on the resting resistance and is the slope of the line created by plotting the change in resistance ($\Delta R/R_0$) of the cPLA strain sensor against the recorded strain from the

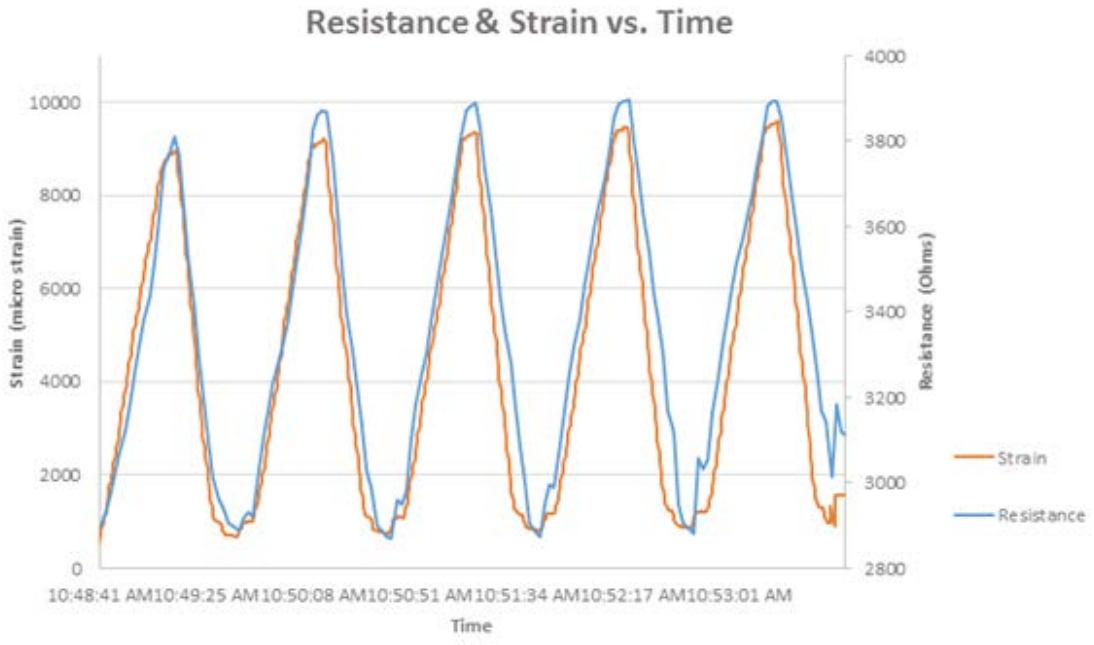

Figure 10: Strain gauge strain and resistance of cPLA strain sensors show similar response under a 5-cycle tensile test. This particular graph is from Sample 4.

commercial strain gauge. This GF value was derived using only the first cycle data per sample for this study. Examples of these plots are Figure 11 and Figure 12 where the loading and unloading resistance-strain curves are independently linearly-fit. Percent linearity error is also measured and was calculated by first determining the line of best fit for one loading cycle, and using this line to intersect the data points with the highest and lowest offset. The vertical offset between these two lines is calculated and then divided by the total vertical span of the data set, and finally expressed as a percent. A smaller value of linear percent error would mean that the deviation of all of the sample points from the linear fit is minimal. The next value calculated is the hysteresis, as most plastic materials experience hysteresis to some extent. Hysteresis, in this study, was calculated by using the two best-fit lines through the loading and unloading data sets separately for a given cycle. From these two best-fit lines, two

vertical offsets were obtained: one offset at the maximum strain, and other offset at the minimum strain. The offset values were each divided by the total vertical span of the data and finally multiplied by 100 to obtain percent values. Although hysteresis is typically measured at the largest strain, this was also measured at the lowest strain because most tests showed a greater offset of resistance at the point where the coupon is finished with the cycle test. This is an example of where the vertical offset of the two best-fit lines are largest at low strain. Finally, a more qualitative approach was taken by visually inspecting the GF and reporting the quality.

There were only two coupons tested from Rostock on the sample matrix, which happens to be a surface printed strain sensor, i.e. not embedded. The linearity percent errors and hysteresis values were the lowest in this study, and the hysteresis values were also relatively low. A few other Rostock coupons were tested, but only have data collected for

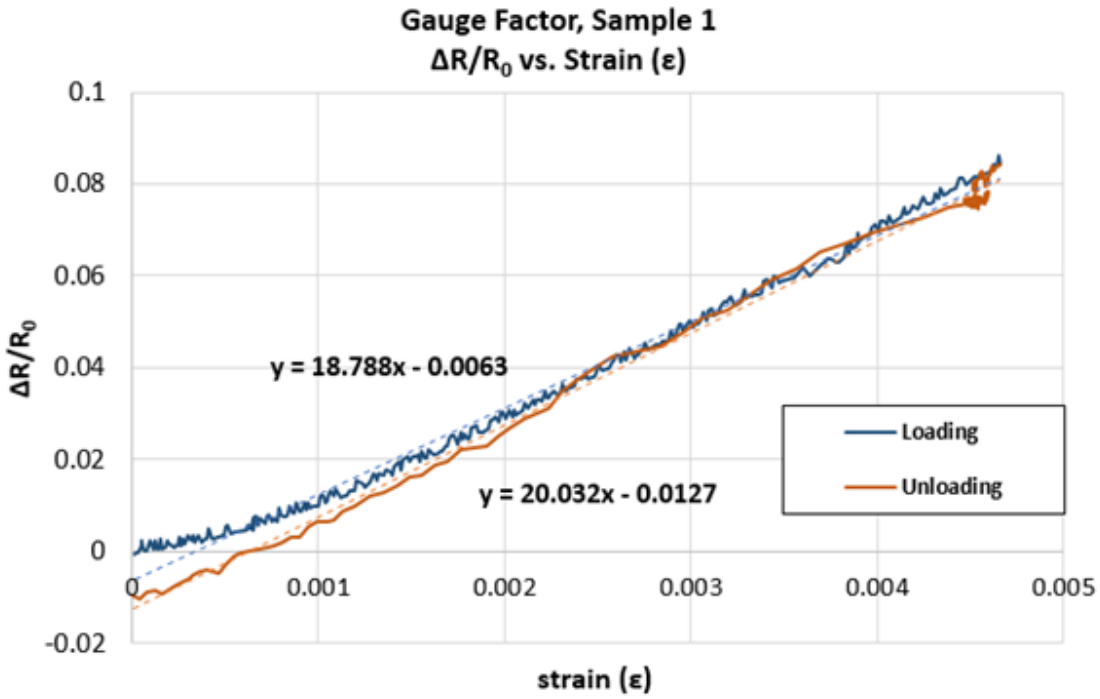

Figure 11: Two linear Gauge Factors (slope) extracted from results for sample 1 printed on the Rostock machine.

the rise in load and thus were not included; however, it is noted that those tests followed a fairly linear path similar to the full Rostock tests for sample 1 and 2.

Also included in Table 2 is the calculated GF from the coupons printed from the TAZ5 and TAZ6 printers with various different print parameters selected. The noticeable difference among these results is that those tested on the MecMesin test stand yielded poorer results and larger error percentages. It is speculated that decline in favorable results is in part due to the strain rate limitation on the MecMesin and that the strain rate was too high for the data acquisition sampling rate of the separate strain and resistance measurements. Since they are not triggered at exactly the same time, there is inherently some timing mismatch (up to half a second) and, therefore, the more dynamic the testing is, the more likely that the results

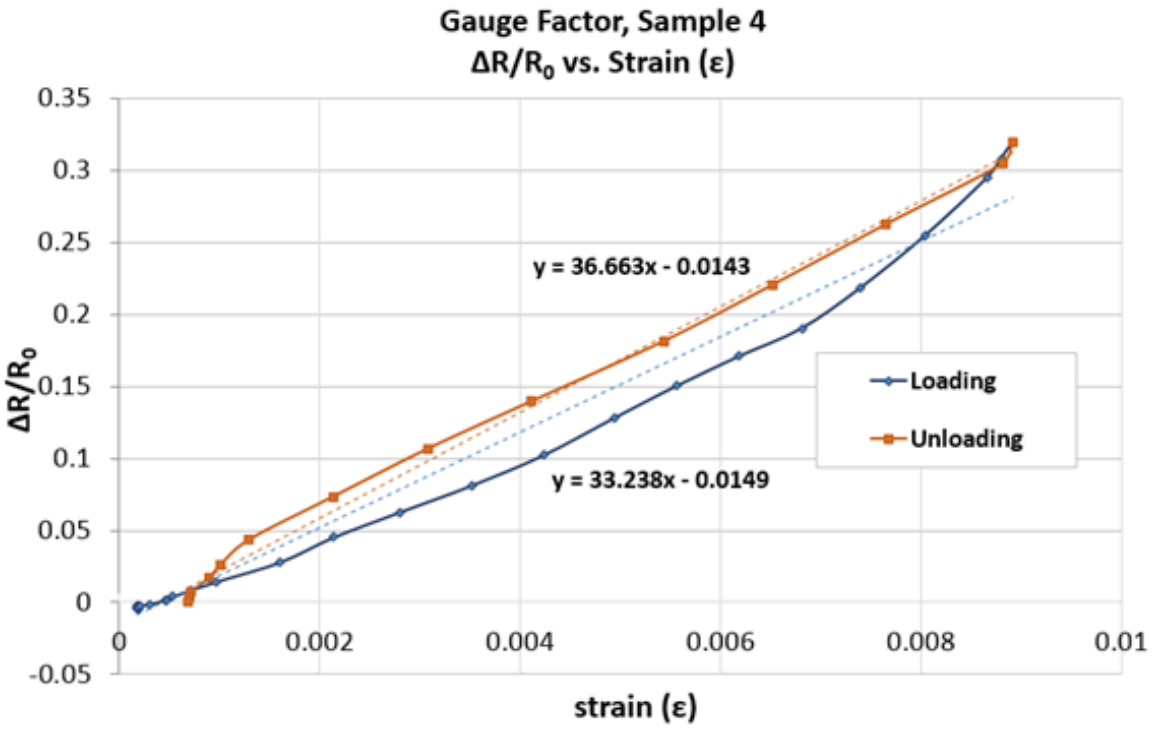

Figure 12: Linear Gauge Factors (slope) extracted from results for sample 4 printed on the TAZ 5 AM machine.

show this time-match error. It is noted in Gooding's research [2] that they encountered the same timing offset, and used the max resistance and maximum strain to align the data.

Those samples tested with the lower strain rates yielded better results. This is not to state that the strain sensor result values are strain dependent, but that the measurement limitations in this study are more apparent at higher rates. If faster strain-rate testing is desired, a better method of triggering measurements of strains and resistances is required.

One of the key indications of a well-designed strain sensor is that the error in linearity is low. By sorting the data from all of the samples by linear error percentage, no particular parameter or sets of parameters are apparent for the cause of lower or higher values. Averages were taken of the GF, linearity and hysteresis values to see whether a pattern emerged, with the results displayed in Table 3. Although multiple samples for each print profile could be created

and tested (similar to sample set 5, which were all printed the same parameters), the following are the findings by reviewing the results table:

1) Although one coupon was created for the I-shaped strain sensor (sample 8) it performed very poorly by visual inspection as well as linearity error. This coupon was omitted from the rest of result of the average calculations in this section.
2) The two Rostock samples, 1 and 2, performed the best. Relative to the samples printed from the TAZ 5 and TAZ 6 printers, the average GF was higher, and all percentage errors were lower in the Rostock samples.
3) Overall the samples printed using the TAZ 6 and TAZ 5 performed similarly, while the TAZ 6 slightly outperformed the TAZ5.
4) The gauge factor (GF) on all samples were much higher than those from the commercial strain gauge. The average GF for all "S" type strain sensors was 19.95, which is about almost 10 times as sensitivity as the commercial strain gauges with a GF=2.06.
5) A trend was established for print speeds. For the print speeds studied in this experiment, the sample data was reviewed for low, medium, and high speeds and found that increasing print speeds increased decreased the GF, and increased linearity errors and both hysteresis values, thus printing at lower speeds is optimal for sensor design. These results can be compared to finding from Muth et al.[7] which found that sensitivity to strain (GF) increased with print speed. Although it is not stated, the graphs from Muth et al.[7] paper shows increasing linearity error for increase speeds, which does correspond to the findings in this thesis.

6) Two print layer heights were chosen for this study. When compared, sample printed with the smaller layer height of 0.2mm resulted in a strain sensor with smaller errors. The GF increased slightly with the larger layer height, but a larger GF may not be indicative of a better sensor.

7) No determination was made between the increase in cPLA nozzle temperature and performance of the strain sensor. Nozzle temperatures that were hotter or cooler than the average temperature of this study performed worse on GF, and hysteresis, while the mid-range temperatures performed the best. Linearity improved with the lowest temperature setting. Many factors are potentially involved when varying temperatures: carbon particulate flow and alignment, overall filament flow, and polymer chain interactions.

Table 2: Resting resistance, calculated GF, linearity, and hysteresis values for tested coupons

Sample #	Organizing group SET	Machine Tested	Starting resistance	1st Cycle GF	Linearity Error %	Hysteresis % Low Strain	Hysteresis % High Strain	Visual Review of GF Plots
1	1	Mark 10	3410	18.93	16.0	7.4	0.7	very good
2	1	Mark 10	3137	17.32	33.0	12.9	14.8	good
3	2	MecMesin	6763	59.25	43.0	17.4	25.3	med-poor
4	2	MecMesin	2887	34.15	17.7	8.5	12.4	good
5	2	MecMesin	2990	36.28	56.7	32.3	16.3	poor
6	2	MecMesin	5045	56.41	91.9	68.7	18.4	poor
7	2	MecMesin	5199	40.35	45.9	22.9	14.0	med-poor
8	3	MecMesin	1212	117.01	86.0	84.0	12.4	very poor
9	4	MecMesin	5364	21.09	47.2	16.0	19.8	medium
10	4	MecMesin	5339	18.53	33.8	105.0	24.6	medium
11	4	MecMesin	1359	14.14	33.7	28.5	41.7	medium
12	4	MecMesin	3094	16.32	27.3	2.7	1.8	good
13	4	MecMesin	4106	10.22	68.9	6.3	4.1	poor
14	4	MecMesin	3823	11.35	54.6	34.5	28.6	med-poor
15	4	MecMesin	7762	6.00	48.5	39.6	14.5	med-poor
16	5	Mark 10	5452	11.54	26.8	5.4	5.3	good
17	5	MecMesin	6653	10.18	37.8	18.9	12.0	med-good
18	5	Mark 10	6456	14.63	52.4	13.5	12.6	medium
19	5	Mark 10	4898	15.38	46.5	38.0	5.3	medium
20	6	Mark 10	6787	7.30	34.3	0.0	21.3	med-good
21	6	Mark 10	8863	9.86	66.2	55.0	12.7	medium
22	6	Mark 10	9987	6.39	44.9	20.4	19.6	good
23	6	Mark 10	8540	9.36	70.0	41.0	20.7	medium
24	6	Mark 10	6893	9.13	41.0	23.5	8.7	med-good
25	6	Mark 10	10432	9.95	31.3	20.6	0.1	good
26	6	Mark 10	9331	16.22	18.7	1.4	9.5	good
27	6	Mark 10	8865	19.48	39.4	20.1	17.1	good
28	6	Mark 10	15204	20.44	97.2	14.8	8.9	med-poor
29	6	Mark 10	20189	38.34	29.2	8.9	14.1	good

Table 3: Evaluations of results from tension tests based on select parameters.

Parameter of Interest	Average GF	Avg. Linearity (% error)	Avg. Hysteresis Low strain (%)	Avg. Hysteresis High strain (%)
Rostock	18.13	24.48	10.15	7.75
TAZ 5	40.70	48.46	27.96	17.44
TAZ 6	14.09	45.23	24.48	14.43
Mark 10 Stand	14.95	43.13	18.86	11.43
MecMesin Stand	25.72	46.69	30.87	17.96
High print speed	9.25	55.50	32.25	14.70
Med print speed	22.05	47.89	23.20	12.68
Low print speed	27.93	27.67	9.78	12.58
"NA" print speed	13.95	44.86	33.23	19.30
Nozzle 2 temp high	45.31	51.04	29.96	17.28
Nozzle 2 temp med	13.07	43.70	19.53	11.29
Nozzle 2 temp low	21.68	34.24	32.22	20.40
Layer height 0.2 mm	20.60	41.65	21.86	13.83
Layer height 0.25 mm	24.60	51.85	36.18	16.85
Starting resistance low	19.85	38.48	16.64	15.05
Starting resistance med	24.53	46.17	30.74	16.78
Starting resistance high	16.25	49.61	22.78	12.84
Set 1	18.13	24.48	10.15	7.75
Set 2	45.31	51.04	29.96	17.28
Set 3	117.01	86.00	84.00	12.40
Set 4	13.95	44.86	33.23	19.30
Set 5	12.93	40.90	18.94	8.80
Set 6	14.65	47.22	20.57	13.27

4.1.3 Strain Rate Dependence on GF

Although the previous section mentions the concerns of the MecMesin load frame's high strain rate, it was also important to investigate if small changes in the applied strain rate of the testing would affect the GF and other stability measurements. Coupon sample # 24 was picked to perform the same tensile loading and unloading testing with varied strain rates. The strain rates performed were 0.5 mm/min, 1 mm/min, 2 mm/min, 3 mm/min, and 5 mm/min. As the five plots show in Figure 13, with increase in strain rate, the determined GF increases, but so does the offset between the loading and unloading data sets which contributes to both

hysteresis and linearity errors. As noted throughout this paper, the time-dependent material response and bonds between the carbon black filler are likely factors contributing to the shift in results at higher strain rates.

Figure 13: Sample #24 tested at varying strain rates shows similar behavior for low strain, but overall GF plot deteriorates for larger strain rates.

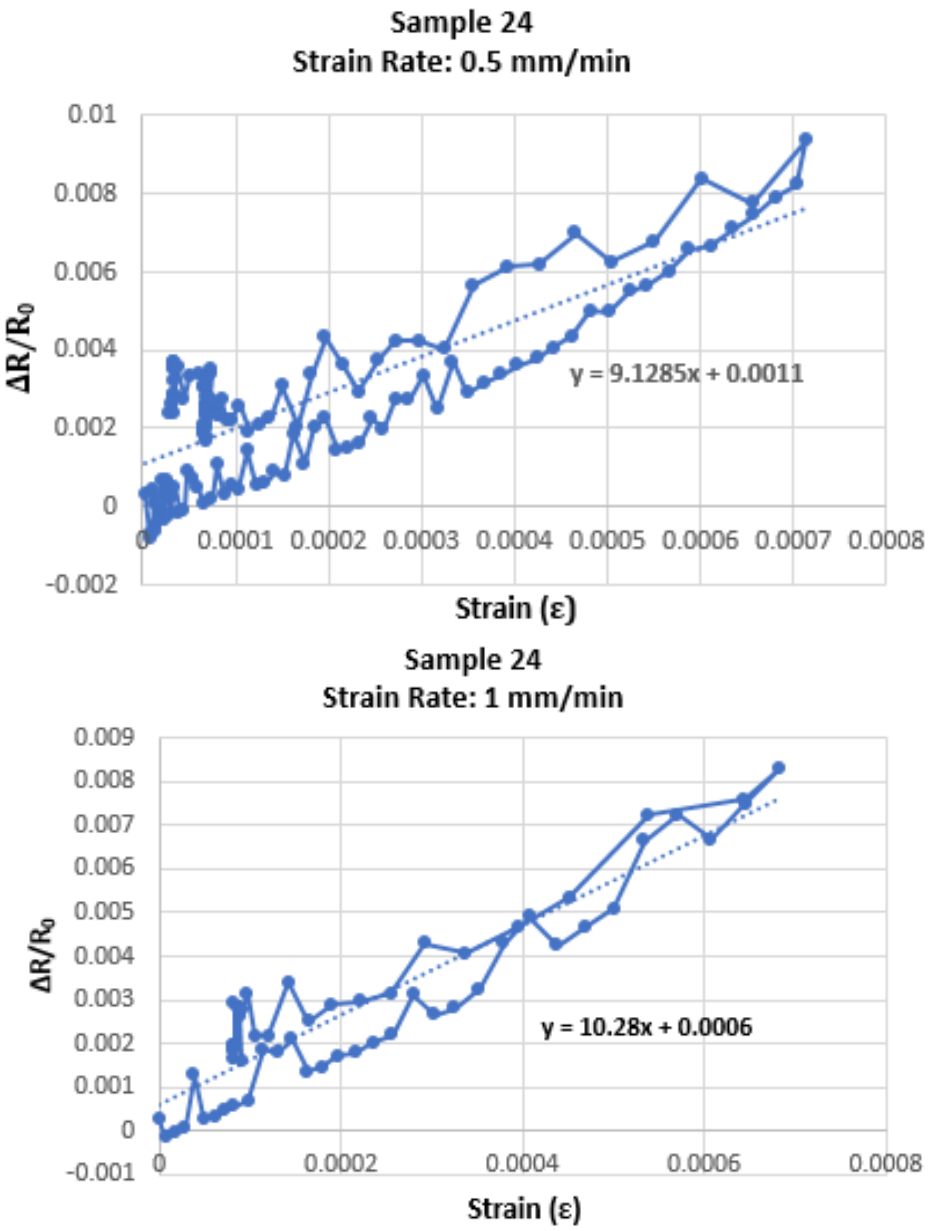

Figure 13: Sample #24 tested at varying strain rates shows similar behavior for low strain, but overall GF plot deteriorates for larger strain rates. Continued.

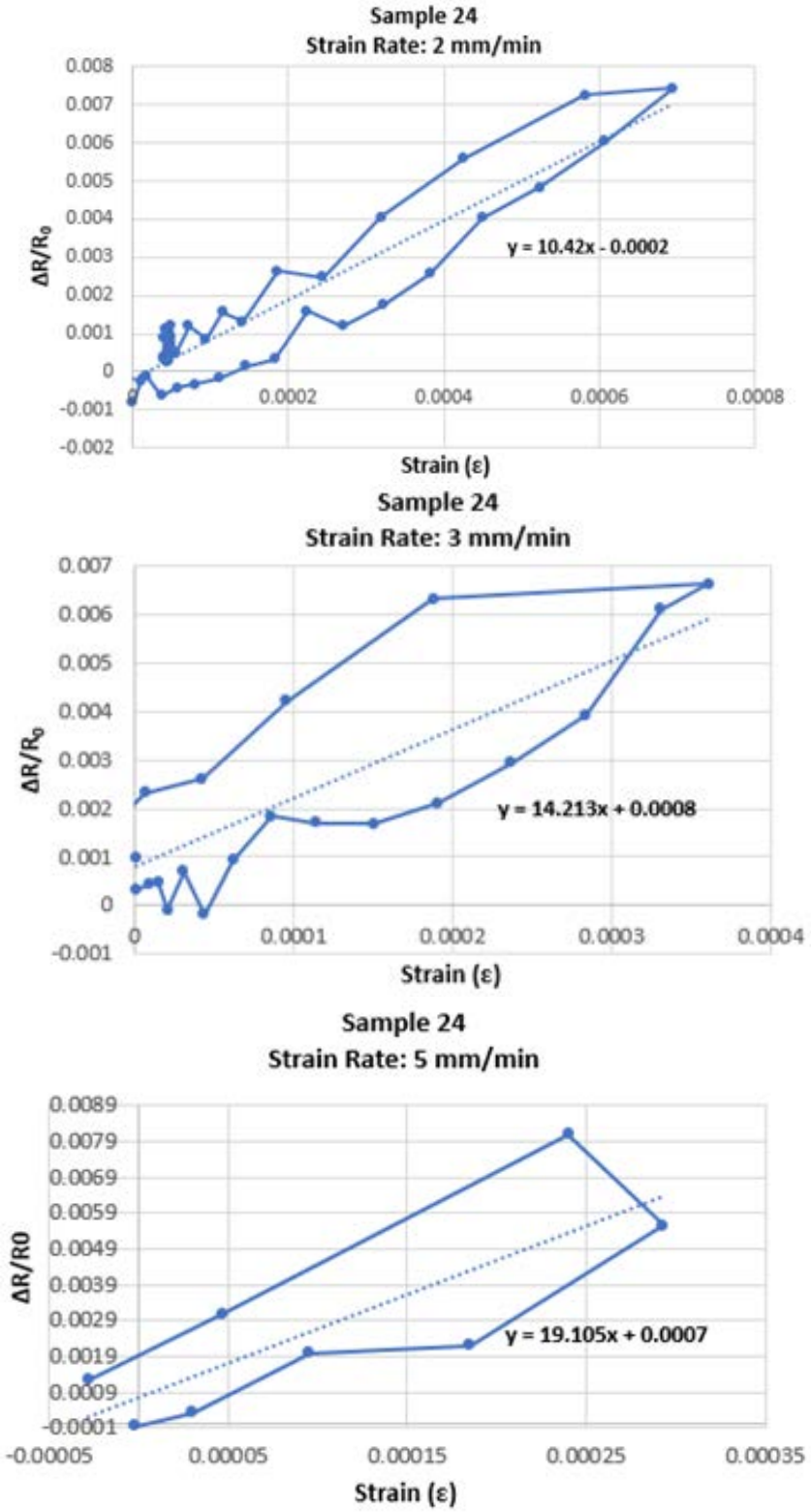

4.1.4 Gauge Factor and Transverse Load Sensitivity

Commercial linear strain gauges are designed to be most sensitive to strain in one direction. This is accomplished by the design of gauge: most of the wire in the gauge is along the direction of intended strain measurement, and only a small percentage of the wire is necessary for the end loops. It would be advantageous to design the conductive strain sensor to mimic the same ratio of cPLA material printed along and perpendicular to the direction of loading. Given the overall design footprint of the strain sensor, the sensor design is limited to the resolution of the 3D printer and thus, only a small number of loops can possibly be printed. For this reason, it is important to determine the strain sensor's sensitivity to transverse loads.

A select number of samples were tested to review the sensitivity to load in the transverse direction. The sample coupons were rotated 90 degrees and gripped on the side edges of each sample. The transverse tension test was performed similarly to those for the longitudinal tests, but the load was stopped around 50-60 N, about a third to half the load of the longitudinal tests. The results of these three tests are shown in Figure 14. The behaviors of all three samples are slightly different, but all show a lower degree of sensitivity toward transverse loading. This is noted by the lower values of slope derived from the data sets shown in Figure 14.

All three strain sensors show low resistance change in the transverse directions when compared to longitudinal loading. Sample 23 shows very low sensitivity. Sample 21 includes unloading data points and has an overall low sensitivity to transverse loading. In order to better evaluate the sensitivity to transverse loading, a separate sample geometry is recommending with enough material to properly grip onto the test coupon. With low

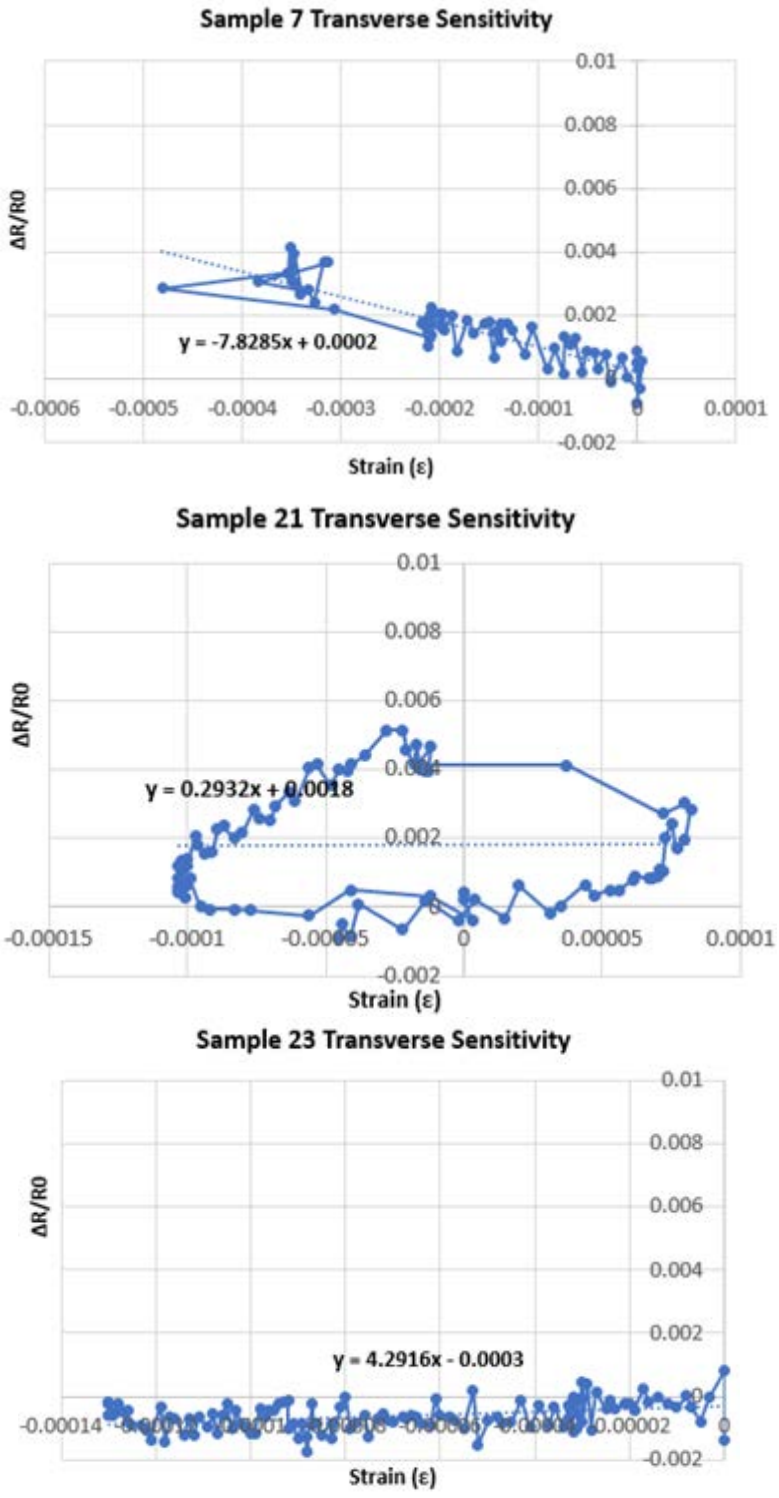

Figure 14: Results from transverse sensitivity tests plotted above for sample 7 (top), sample 21 (middle) and sample 24 (bottom).

resistance change during these tests, one would also need to control or remove temperature effects from the results.

4.2 Basic Stiffness Comparison Results

A small suite of tests were performed to evaluate the tensile stiffness of several PLA coupons: some with a cPLA strain sensor printed on the surface, some with the strain sensor embedded into the coupon, and some without any sensor attached. These findings are shown in Figure 15, and suggest that the behavior of the sample with the embedded sensor is similar and is within the results of the coupons that do not contain embedded sensors. Additional material testing is currently in progress to quantify material properties of both the PLA and cPLA materials used in this experiment.

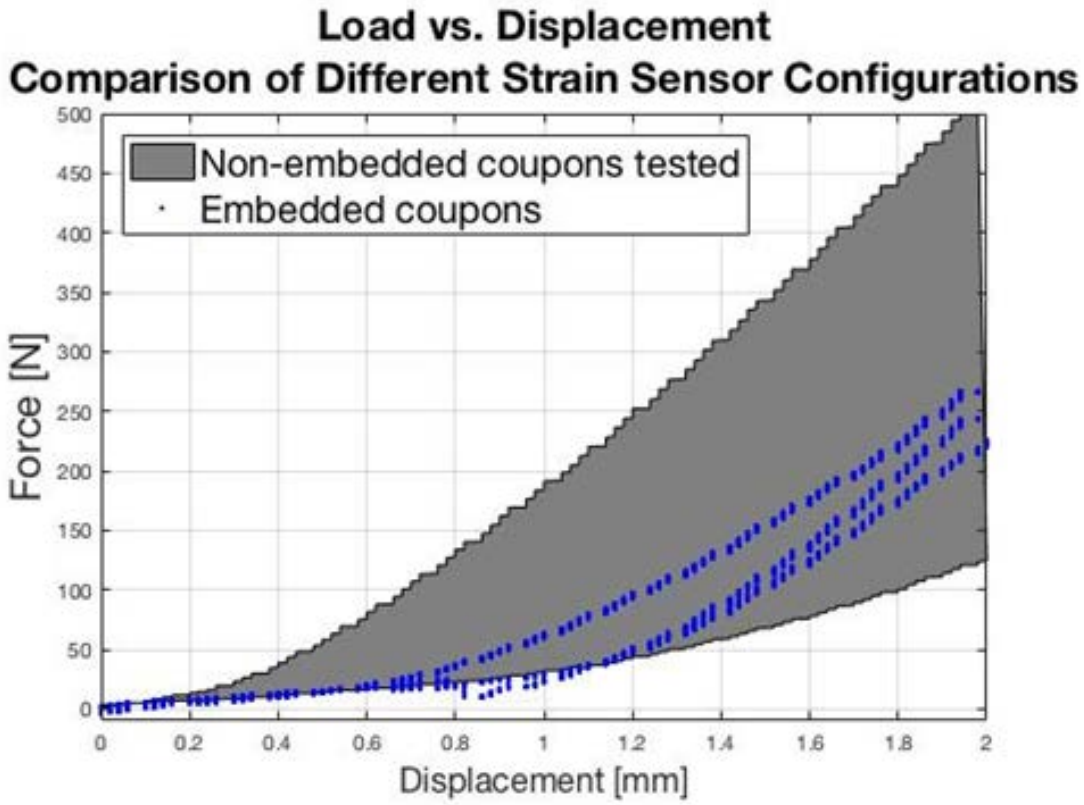

Figure 15: Load vs. Displacement results for various configuration types. The blue dotted-plots are three embedded coupons and show that they respond within the range of the other non-embedded strain sensor coupons.

4.3 Temperature- Resistance Comparison Results

Another observation that was obtained from recording nominal resistance values for test coupons was a small percent fluctuation in resistance over time. Initially, it was hypothesized that the fluctuations may be due to sensor self-heating. A longer duration test was implemented to record nominal resistance values along with readings from a temperature monitor. Plotted against the time on the x-axis, the resistance and temperature responses for sample 20 lined up extremely well as shown in Figure 16. Two other samples (Sample # 13 and 24) were tested in the same manor and showed a similar temperature related behavior. The temperature effects on the strain sensor resistance readings were also investigated, and more details can be found in

the manuscript by Wahry et al. [13]. Noting that temperatures have an effect on resistance measurements, the thermal effects on resistance must be either subtracted from the collected data by way of a secondary non-loaded strain sensor operating in the same thermal environment, or by performing the tests in a controlled temperature environment. Samples 19 and 23 have similar resting resistances, which are larger than sample 13.

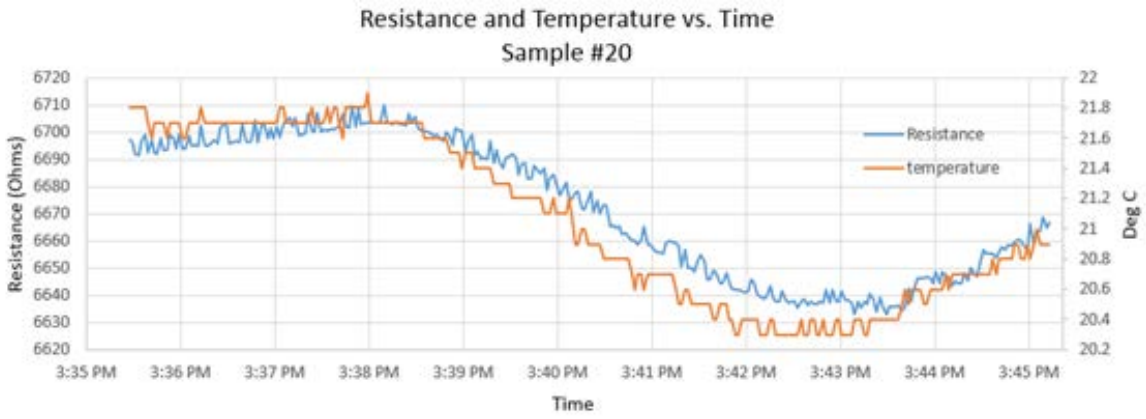

Figure 16: Resistance measurements and room temperature recordings over a 10-minute span.

Table 4: Summary of room temperature resistance fluctuations. The right most column shows the sensitivity of the strain sensor normalized by one degree change in temperature.

Sample Number	Largest ΔT (°C)	ΔR (Ohms)	Time Duration (h/m/s)	ΔR/ °C
20	1.6	75	0:05:05	46.88
13	1.5	31	0:03:24	20.67
24	0.7	32	0:04:20	45.71

4.4 Strain Dependencies Based on AM Part Surfaces

Independent of sample orientation in both test stands, the surface of the sample that was first printed is referred to as the build plate side. All samples printed from the TAZ machines all had a similar trait in that the build plate side appeared less opaque and was smoother than the non-build plate side. Photos taken of each side of a sample show the general surface finish for the TAZ samples.

The test with two strain gauges confirmed that there was a difference in strain recorded for each side of the sample. The DIC results confirmed that slightly more deformation along the length of the coupon occurs on side 1 (the build-plate surface), than on side 2 (free surface). These results match several tests of coupons with strain gauges on both sides, tested on both the Mark-10 and MecMesin test stands; however, some instances showed the side opposite the print bed straining more than the other. Using DIC images, as opposed to strain gauges, provided a couple advantages. The first advantage of DIC is that the results are not dependent on the bond of the commercial strain gauge to the specimen, and thus inaccuracies due to bond layer thickness or failed bond contact areas are not incorporated into the DIC results. Secondly, DIC allows the user to view strain fields of almost the full field of view, or captured speckle pattern. This gives the user insight of high or low strain fields that may be located outside the strain gauge footprint.

A video of the DIC results shows the behavior of the coupon during loading and unloading; high strain values are concentrated around the conductive attachment pads, but this is likely to be missed by the commercial strain gauge. A Region of Interest (ROI) was mapped in the software to represent the commercial strain gauge footprint, and longitudinal strains were calculated and graphs were exported that plot longitudinal strains against the number of images

that span the tension loading and unloading. This was done for each coupon side and compared. Side 1 shows more strain for the same peak load and load profile.

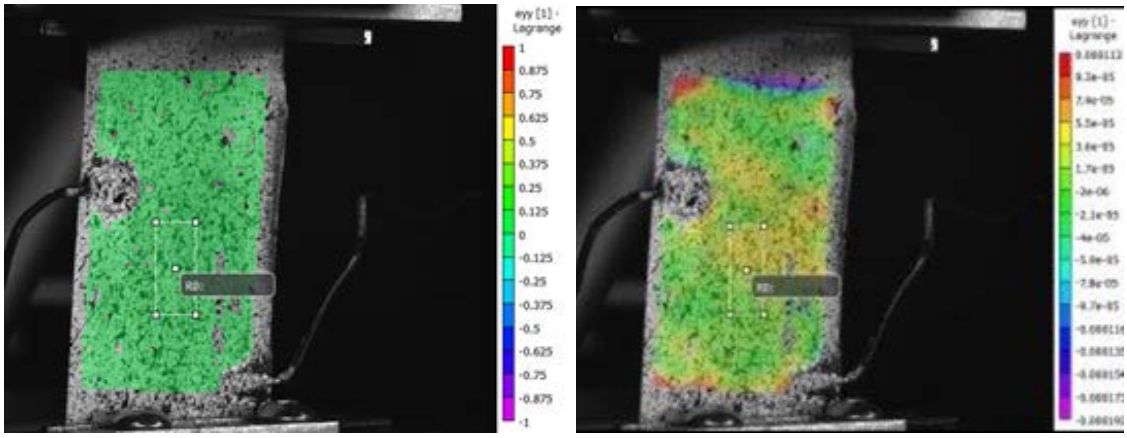

Figure 17: DIC Post-processing images of side 1. (left) images shows the initial image taken prior to testing. Included in this image is the Region of Interest (ROI) where strain measurements can be exported. (right) The contour plot of strain in the longitudinal direction (ε_{yy}).

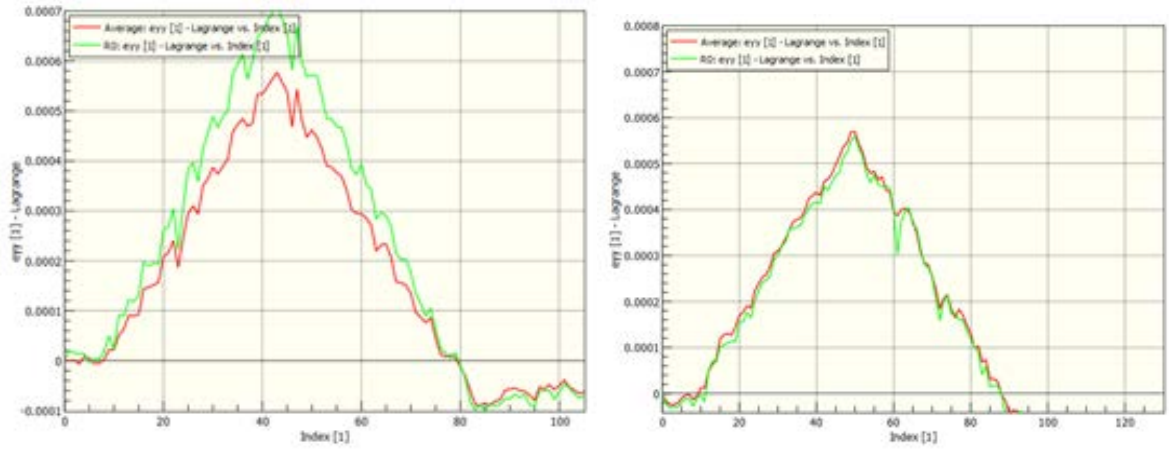

Figure 18: Post-processed results from side 1 (left) and side 2 (right). The green plot is the longitudinal strain in the ROI, and the red plot contains averaging of the longitudinal strains. Although the max strain from the average data is similar on both sides, side 1 shows more strain than side 2.

Although these results indicate more complex behavior of 3D printed parts, this thesis paper is more focused on understanding the behavior of the cPLA resistance to strain. An

additional study investigating print direction strains is recommended. To better understand the behavior of AM parts under loading, it is suggested to use more samples of the same print parameters with an additional set of cameras such that both sides of the sample can used DIC for the same load test.

The Abstract, and Chapter 1 through 4, in part, has been published in the manuscript. 11th International Workshop on Structural Health Monitoring 2017. Rumley-Ouellette, Brittany J., Wahry, J., Baker, A., Bernardin, J, Marchi, A., Todd, M. The thesis author was the primary investigator and author of this paper.

Chapter 5

Conclusion

5.1 Overview

The studies presented in this thesis contribute to the development of in-situ strain sensors comprised of similar polymer-based materials for AM parts. This research also reviewed the effects of varying common FDM user-selectable parameters. In summary, the conductive strain sensors in this study had an average GF of 19.95, which makes the cPLA strain sensors about 10 times more sensitive than the commercial linear strain sensors used in the experimental section of this work. The strain sensors printed from the Rostock outperformed those printed from the TAZs when reviewing linearity and hysteresis errors. Although not one particular variable was responsible for enhanced or lessened quality of the sensor, a trend was observed for print speed: an increased print speed yields a lower GF and higher linearity and hysteresis errors. A definitive trend was not observed for nozzle temperature result values, however linearity error decreased as nozzle temperature decreased. Samples printed using a layer height of 0.2mm instead of 0.25 mm resulted in lower errors for linearity and hysteresis.

Although several parameters were reviewed, most showed little influence on the GF, linearity and hysteresis of the strain sensor design. Samples printed from the Rostock AM printer performed better than the TAZ samples.

This research also investigated several other interesting behaviors of embedded conductive filament in additively manufactured parts. First, the relationship between measured sensor resistance and small changes in the laboratory temperature were noticed. Although this

was investigated in-depth in a separate project, it was observed that small fluctuations in the resistance of a resting strain sensor were closely correlated to the surface temperature of the sample. Second, sensor sensitivity to transverse loading was explored, and found to be approximately 1/5 the sensitivity as the longitudinal direction, although a more controlled study is suggested. Finally, testing using strain gauges bonded on both sample sides as well as DIC, revealed a dissimilarity in surface strains under longitudinal tension loading.

5.2 Future Research

Future work related to this study is required in order to use FDM printed strain sensors in AM parts. Samples from set 5 were printed using the same parameter values, yet the GF, linearity and hysteresis values varied between them. Understanding other causes to the print variability of the TAZ machines, and variability in sample assembly is required prior to using FDM printed sensors for accurate strain measurements in parts. Investigation into lead wire insertion variability, and improved methods of strain measurements (DIC) along with higher sampling rates are among the top improvements. An investigation into understanding the strain discrepancies between each surface of AM coupons is currently underway and will use two sets of cameras to obtain data from both sides of the sample during one test.

APPENDIX

Table 5: Full review of print parameters and results

Sample #	Organizing Group SET	Machine Tested	Starting resistance	1st Cycle GF	Linearity Error %	Hysteresis % Low Strain	Hysteresis % High Strain	Visual Review of GF Plots	Printer	Layer Height (mm)	Nozzle 1 Temp (°C)	Nozzle 2 Temp (°C)	Build Plate Temp (°C)	Print Speed (mm/sec)	density (%)	Flow (%)	Nozzle 1 diameter change	Nozzle 2 diameter change
1	1	Mark 10	3410	18.93	16.0	7.4	0.7	very good	Rostock	0.2	210	210	60	40	100	NA	None	None
2	1	Mark 10	3137	17.32	33.0	12.9	14.8	good	Rostock	0.2	210	210	60	40	100	NA	None	None
3	2	MecMesin	6763	59.25	43.0	17.4	25.3	med-poor	TAZ 5	0.2	208	215	70	20	70	100	None	None
4	2	MecMesin	2887	34.15	17.7	8.5	12.4	good	TAZ 5	0.2	208	215	70	50	70	100	None	None
5	2	MecMesin	2990	36.28	56.7	32.3	16.3	poor	TAZ 5	0.2	208	215	70	50	70	100	None	None
6	2	MecMesin	5045	56.41	91.9	68.7	18.4	poor	TAZ 5	0.2	208	215	70	50	70	100	None	None
7	2	MecMesin	5199	40.35	45.9	22.9	14.0	med-poor	TAZ 5	0.2	208	215	70	50	70	100	None	None
8	3	MecMesin	1212	117.01	86.0	84.0	12.4	very poor	TAZ 5	0.2	208	215	70	50	70	100	None	None
9	4	MecMesin	5364	21.09	47.2	16.0	19.8	medium	TAZ 6	0.25	208	205-208	50	NA	70	100	None	None
10	4	MecMesin	5339	18.53	33.8	105.0	24.6	medium	TAZ 6	0.25	208	205-208	50	NA	70	100	None	None
11	4	MecMesin	1359	14.14	33.7	28.5	41.7	medium	TAZ 6	0.2	208	208	50	NA	70	100	None	None
12	4	MecMesin	3094	16.32	27.3	2.7	1.8	good	TAZ 6	0.2	208	208	50	NA	70	100	None	None
13	4	MecMesin	4106	10.22	68.9	6.3	4.1	poor	TAZ 6	NA	NA	NA	NA	NA	NA	100	None	None
14	4	MecMesin	3823	11.35	54.6	34.5	28.6	med-poor	TAZ 6	NA	NA	NA	NA	NA	NA	100	None	None
15	4	MecMesin	7762	6.00	48.5	39.6	14.5	med-poor	TAZ 6	NA	NA	NA	NA	NA	NA	100	None	None
16	5	Mark 10	5452	11.54	26.8	5.4	5.3	good	TAZ 6	0.2	210	210	32/NA	50	NA	100	3.35	None
17	5	MecMesin	6653	10.18	37.8	18.9	12.0	med-good	TAZ 6	0.2	210	210	32/NA	50	NA	100	3.35	None
18	5	Mark 10	6456	14.63	52.4	13.5	12.6	medium	TAZ 6	0.2	210	210	32/NA	50	NA	100	3.35	None
19	5	Mark 10	4898	15.38	46.5	38.0	5.3	medium	TAZ 6	0.2	210	210	32/NA	50	NA	100	3.35	None
20	6	Mark 10	6787	7.30	34.3	0.0	21.3	med-good	TAZ 6	0.2	210	210	33	50	70	100	3.35	None
21	6	Mark 10	8863	9.86	66.2	55.0	12.7	medium	TAZ 6	0.2	210	210	33	50	70	100	3.35	None
22	6	Mark 10	9987	6.39	44.9	20.4	19.6	good	TAZ 6	0.2	210	210	33	50	70	100	3.35	None
23	6	Mark 10	8540	9.36	70.0	41.0	20.7	medium	TAZ 6	0.2	210	210	33	70	70	100	3.35	None
24	6	Mark 10	6893	9.13	41.0	23.5	8.7	med-good	TAZ 6	0.2	210	210	33	70	70	100	3.35	None
25	6	Mark 10	10432	9.95	31.3	20.6	0.1	good	TAZ 6	0.2	215	210	33	50	70	90	3	2.75
26	6	Mark 10	9331	16.22	18.7	1.4	9.5	good	TAZ 6	0.2	212	210	33	20	70	90	3	2.75
27	6	Mark 10	8865	19.48	39.4	20.1	17.1	good	TAZ 6	0.2	212	210	33	50	70	90	3	2.75
28	6	Mark 10	15204	20.44	97.2	14.8	8.9	med-poor	TAZ 6	0.25	212	210	33	50	70	90	3	2.8
29	6	Mark 10	20189	38.34	29.2	8.9	14.1	good	TAZ 6	0.25	210	205	33	50	70	90	3	2.85

REFERENCES

[1] Baker, A.M., Mccoy, J., Majumdar, B.S., Rumley-Ouellette, B., Wahry, J., Marchi, A.N., Bernardin, J.D. and Spernjak, D. 2017. Measurement and Modelling of Thermal and Mechanical Anisotropy of Parts Additively Manufactured using Fused Deposition Modelling (FDM). *11th International Workshop on Structural Health Monitoring 2017* (Stanford University, 2017).

[2] Gooding, J. and Fields, T. 2017. 3D Printed Strain Gauge Geometry and Orientation for Embedded Sensing. (Grapevine, Texas, Jan. 2017).

[3] Jeong, Y.R., Park, H., Jin, S.W., Hong, S.Y., Lee, S.-S. and Ha, J.S. 2015. Highly Stretchable and Sensitive Strain Sensors Using Fragmentized Graphene Foam. *Advanced Functional Materials*. 25, 27 (Jul. 2015), 4228–4236. DOI:https://doi.org/10.1002/adfm.201501000.

[4] J. Martinez, J.L. Dieguez, E. Ares, A. Pereira, P. Hernandez and J.A. Perez 2013. Comparative between FEM Models for FDM Parts and their Approach to a Real Mechanical Behaviour. *Procedia Engineering* (Zaragoza, Spain, Jan. 2013), 878–884.

[5] J.S. Bergstrom and M.C. Boyce 1998. Constitutive modeling of the large strain time-dependent behavior of elastomers. *Journal of the Mechanics and Physics of Solids*. 46, 5 (May 1998), 931–954. DOI:https://doi.org/10.1016/S0022-5096(97)00075-6.

[6] Kost, J., Foux, A. and Narkis, M. 1994. Quantitative model relating electrical resistance, strain, and time for carbon black loaded silicone rubber. *Polymer Engineering & Science*. 34, 21 (Nov. 1994), 1628–1634. DOI:https://doi.org/10.1002/pen.760342108.

[7] Muth, J.T., Vogt, D.M., Truby, R.L., Mengüç, Y., Kolesky, D.B., Wood, R.J. and Lewis, J.A. 2014. Embedded 3D Printing of Strain Sensors within Highly Stretchable Elastomers. *Advanced Materials*. 26, 36 (Sep. 2014), 6307–6312. DOI:https://doi.org/10.1002/adma.201400334.

[8] OMEGA pre-wired Strain Gauges: *https://www.omega.com/pptst/KFH.html*. Accessed: 2018-01-29.

[9] Park, Y.-L., Tepayotl-Ramirez, D., Wood, R.J. and Majidi, C. 2012. Influence of cross-sectional geometry on the sensitivity and hysteresis of liquid-phase electronic pressure sensors. *Applied Physics Letters*. 101, 19 (Nov. 2012), 191904. DOI:https://doi.org/10.1063/1.4767217.

[10] R. Sbriglia, L., Baker, A., M. Thompson, J., V. Morgan, R., J. Wachtor, A. and D. Bernardin, J. 2016. Embedding Sensors in FDM Plastic Parts During Additive Manufacturing. *Proceedings of the 34th IMAC, A Conference and Exposition of Structural Dynamics 2016* (Jan. 2016), 205–214.

[11] Ruge, A.C. 1944. Strain gauge. US2340146 A. Jan. 25, 1944.

[12] Stübler, N., Jungk, J. and Klueppel, M. 2011. Mechanical and Electrical Analysis of Carbon Black Networking in Elastomers Under Strain. *Polymer Engineering & Science*. 51, (Jun. 2011), 1206–1217. DOI:https://doi.org/10.1002/pen.21888.

[13] Wahry, J., Rumley-Ouellette, B.J., Todd, M. and Marchi, A. 2017. Conductive Poly Lactic Acid (PLA) Temperature Sensors Embedded in Additively Manufactured Parts. *11th International Workshop on Structural Health Monitoring 2017* (Stanford University, 2017).

[14] Wei, L.-J. 2015. *The Fabrication of Integrated Strain Sensors for "Smart" Implants using a Direct Write Additive Manufacturing Approach*. De Montfort University.

[15] Wei, L.-J. and Oxley, C.H. 2016. Carbon based resistive strain gauge sensor fabricated on titanium using micro-dispensing direct write technology. *Sensors and Actuators A: Physical*. 247, Supplement C (Aug. 2016), 389–392. DOI:https://doi.org/10.1016/j.sna.2016.06.025.

[16] 2017. AN1701- Speckle Pattern Fundamentals.